

Aeroelastic Stability of Trailing-Edge Flap Helicopter Rotors

Jinwei Shen

Inderjit Chopra

Graduate Research Assistant

Alfred Gessow Professor and Director

Alfred Gessow Rotorcraft Center,

Department of Aerospace Engineering

University of Maryland, College Park, MD 20742

Abstract

This paper investigates the aeroelastic stability of a helicopter rotor blade with trailing edge flaps. The coupled blade/flap/actuator equations were linearized by using small perturbation motions about a steady trimmed solution. Stability is then determined from an eigenanalysis of these homogeneous equations using the Floquet method. The baseline correlation of stability calculations without trailing-edge flaps is carried out with wind tunnel test data for a typical five-bladed bearingless rotor system. Good agreement is seen for both hover and forward flight conditions. Stability calculations for a rotor with trailing-edge flaps were conducted to examine the effect of flap aerodynamic balance and flap mass balance. The effects of various key design variables such as flap overhang length, flap CG offset, rotor control system stiffness, blade torsional stiffness, actuator stiffness, and trailing-edge flap size and location on the aeroelastic stability characteristics of a trailing-edge flap rotor system were also examined in different flight conditions. Excessive flap aerodynamic over-balancing and mass unbalancing are shown to cause instabilities of the trailing-edge flap blade system.

Notation

C_{FF}	Flap damping
C_{FR}	Flap-blade damping vector
C_{RF}	Blade-flap damping vector
C_{RR}	Blade damping matrix
C_d	Sectional drag coefficient
C_h	Sectional flap hinge moment coefficient
C_l	Sectional lift coefficient
C_{lf}	Sectional flap hinge lift coefficient
C_m	Sectional pitch moment coefficient
K_{FF}	Flap stiffness
K_{FR}	Flap-blade stiffness vector
K_{RF}	Blade-flap stiffness vector
K_{RR}	Blade stiffness matrix
M_{FF}	Flap mass
M_{FR}	Flap-blade mass vector
M_{RF}	Blade-flap mass vector
M_{RR}	Blade mass matrix
Q_F	Trailing-edge flap deflection
Q_R	Modal blade displacement vector
R	Rotor radius
c	Blade chord

c_a Flap actuator torsional damping
 c_b Flap overhang length
 c_f Flap chord
 c_{cg} Flap CG offset (positive backward)
 k_a Flap actuator torsional stiffness
 t Time
 α Angle of attack
 δ_a Actuator deflection (positive flap down)
 δ_f Flap deflection (positive flap down)
 δT Variation in kinetic energy
 δU Variation in strain energy
 δW Virtual work

Subscripts

a Actuator
b Blade
f Trailing-edge flap

Other Symbols

$\Delta(\cdot)$ $(\cdot)_n - (\cdot)_{n-1}$, perturbation

$\delta(\cdot)$ Virtual variation

$(\cdot)^*$ $\frac{d}{d\psi}$

$(\cdot)^{**}$ $\frac{d^2}{d\psi^2}$

Introduction

Trailing edge flap systems for rotor blades have received considerable attention by researchers as a highly effective means for vibration reduction (Refs. 1–6), automated in-flight tracking (Ref. 7), and primary flight control (Ref. 8). However, the aeroelastic stability associated with these flap systems is a concern that has received little attention to date. Satisfactory stability characteristics that include blade aeroelastic stability and ground or air resonance (Ref. 9) may be critical to the design.

Flutter phenomena of control surfaces in fixed-wing aircraft, such as wing-aileron, tail-elevator and rudder, are well studied. Many of the theories and practices associated with flutter on flaps of fixed-wing aircraft may also be applicable to rotorcraft, and the current paper will use similar approaches with respect to trailing-edge flaps on rotor blades. Broadbent (Ref. 10) presented a discussion on flutter of control surfaces and tabs. The nature of aeroelastic stability of wing-aileron systems is explained by considering the aerodynamic forces that arise from the aileron motion and solving the binary flutter equations of wing bending-aileron and wing torsion-aileron. It is explained that the avoidance of control surface flutter can be achieved by using mass-balance, irreversible controls, and adding more damping. Fung (Ref. 11) explained the flutter phenomenon by considering energy transfer between wing distortion and aileron deflection, and gave historical remarks on flutter analysis development. Theodorsen (Ref. 12) presented the aerodynamic model for an oscillating airfoil

or airfoil-aileron combination with three independent degrees of freedom: wing bending, wing torsion, and aileron deflection. The calculated stability solution is compared with experimental data, and the comparison shows fair to good agreement.

Compared with control surfaces in fixed-wing aircraft, trailing-edge flap embedded on rotor blades operates in an even more complex aerodynamic and inertial environment, and thus may induce unique aeroelastic instabilities. The objective of this research is to investigate systematically the aeroelastic stability of a rotor system with trailing-edge flaps, and examine the effects of various key design variables such as flap overhang length, flap CG offset, rotor control system stiffness, blade torsional stiffness, actuator stiffness, and trailing-edge flap size and location on the aeroelastic stability characteristics of a trailing-edge flap rotor system.

Analytical Model

The baseline rotor analysis is taken from UMARC (University of Maryland Advanced Rotorcraft Code) (Ref. 13). The blade is assumed as an elastic beam undergoing flap bending, lag bending, elastic twist, and axial deformation. The derivation of the coupled blade/actuator/trailing edge flap equations of motion is based on Hamilton's variational principle generalized for a nonconservative system.

$$\delta\Pi = \int_{t_1}^{t_2} (\delta U - \delta T - \delta W) dt = 0 \quad (1)$$

δU is the variation of the elastic strain energy, δT is the variation of the kinetic energy, and δW is the work done by nonconservative forces. The blade, trailing edge flap, and actuator contribute to the energy expressions:

$$\delta U = \delta U_b + \delta U_f + \delta U_a \quad (2)$$

$$\delta T = \delta T_b + \delta T_f + \delta T_a \quad (3)$$

$$\delta W = \delta W_b + \delta W_f + \delta W_a \quad (4)$$

where the subscripts b , f , and a refer to the blade, trailing edge flap, and actuator respectively.

Structural modeling

The trailing-edge flap actuator is modeled with a torsional spring and damper system that connects the flap with the baseline blade. The flap hinge can be located at an arbitrary chordwise position of the flap. The flap motion is indirectly controlled via base motion of the actuator (Figure 1). The actuator and flap mass is lumped into the baseline blade mass so that the blade sectional structural properties reflect the entire section. The flap is assumed to undergo

the same flap bending, lag bending, elastic twist, and axial deformation as the blade but with an additional degree of freedom - trailing-edge flap deflection. The baseline rotor is the McDonnell-Douglas Advanced Rotor Technology (MDART) system. The MDART rotor is a pre-production MD900 rotor, a modern five-bladed bearingless rotor (Table 1). A bearingless rotor model was employed, featuring multiple load paths for flexbeam/torque tube configuration, viscoelastic snubber, kinematics of control linkage, and nonlinear bending-torsion coupling within the flexbeam (Ref. 14). The main blade, the flexbeam, and the torque tube are each discretized into a finite number of beam elements, each with fifteen degrees of freedom. The flexbeam and torque tube consists of four and three elements respectively. Twelve elements are used for the main blade and one element for the swept tip. Modal reduction using nine blade coupled natural vibration modes is employed to normalize the blade equations of motion.

Aerodynamic modeling

There are several available aerodynamic models for a flapped airfoil. The Hariharan-Leishman model (Ref. 15) is incorporated into UMARC for trailing edge flap studies (Ref. 16). Based on the indicial method, this model includes compressibility and unsteady effects. However, this model assumes the flap hinge located at the nose of flap, and thus lacks the capability to handle an aerodynamically balanced flap (Figure 2). Trailing-edge flap aerodynamic balance (nose overhang) is incorporated to change the aerodynamic characteristics of the airfoil/flap in order to reduce flap hinge moment, and hence actuation power

(Ref. 17). Flap nose overhang is defined as the hinge offset from the leading-edge of the flap in terms of full chord. The baseline MD900 flap system was designed with the flap hinge located at 10% chord behind the flap nose. This translates into an overhang of 29% of flap chord. To model the aerodynamically balanced flap, quasi-steady models adapted respectively from Theodorsen's theory (Ref. 18), and table lookup based on test data are used. Theodorsen's theory does not include the compressibility effect which can be significant in transonic flow. For the second model, the blade aerodynamic section coefficients (C_l , C_d , C_m) and flap aerodynamic coefficients (C_h , C_{lf}) are obtained from the table lookup for specific angles of attack (α), Mach Number (M), and trailing-edge flap deflection (δ_f). For the airfoil without a trailing-edge flap, table lookup is used to define the blade aerodynamic coefficients. The Bagai-Leishman free wake model(Ref. 19) is used to obtain induced inflow distribution on the rotor disk.

Trim Analysis

The coupled blade and trailing-edge flap responses and the trim control settings were solved simultaneously for the wind tunnel trim condition using finite element in time. Eighteen time elements with seventh order shape functions are used to calculate the coupled trim solution. The wind tunnel trim procedure involves adjusting the controls to achieve zero first harmonic blade flapping, with a prescribed thrust level ($C_T/\sigma = 0.075$) and shaft angles. The trim solution and blade/trailing-edge flap responses are updated iteratively until the convergence criteria are reached.

Stability Analysis

The present study is focused on a stability analysis for a flap rotor system using a linearized eigenanalysis method. Linear differential equations are derived for the perturbed motion of the rotorcraft system about the trimmed state. Stability is then determined from an eigenanalysis of these homogeneous equations using the Floquet method.

Rotor-flap perturbation equations are shown below. The blade equations of motions are coupled with flap motion because of aerodynamic and inertial loading on the blade is changed from flap deflection. The flap equation contains the effect of blade motions because they contribute to the calculations of hinge moment which determines the flap motion. The flap matrices include actuator dynamics.

$$\begin{aligned}
 & \text{Rotor : } \begin{bmatrix} \mathbf{M}_{RR} & \mathbf{M}_{RF} \end{bmatrix} \begin{Bmatrix} \Delta \mathbf{Q}_R^{**} \\ \Delta \mathbf{Q}_F^{**} \end{Bmatrix} \\
 & \text{Flap : } \begin{bmatrix} \mathbf{M}_{FR} & \mathbf{M}_{FF} \end{bmatrix} \begin{Bmatrix} \Delta \mathbf{Q}_R^{**} \\ \Delta \mathbf{Q}_F^{**} \end{Bmatrix} \\
 & + \begin{bmatrix} \mathbf{C}_{RR} & \mathbf{C}_{RF} \\ \mathbf{C}_{FR} & \mathbf{C}_{FF} \end{bmatrix} \begin{Bmatrix} \Delta \dot{\mathbf{Q}}_R^* \\ \Delta \dot{\mathbf{Q}}_F^* \end{Bmatrix} \\
 & + \begin{bmatrix} \mathbf{K}_{RR} & \mathbf{K}_{RF} \\ \mathbf{K}_{FR} & \mathbf{K}_{FF} \end{bmatrix} \begin{Bmatrix} \Delta \mathbf{Q}_R \\ \Delta \mathbf{Q}_F \end{Bmatrix} = \mathbf{0} \quad (5)
 \end{aligned}$$

Results and Discussion

Before stability results for the trailing-edge flap rotor are presented, the predictive capabilities of UMARC for a bearingless rotor without trailing-edge flaps are evaluated by correlating with wind tunnel experimental data. The trailing-edge flap hinge moments of UMARC are compared with CAMRAD II predictions. Then the UMARC predictions of stability results for the trailing-edge flap rotor are carried out, and the flap aerodynamic and mass balance effects are investigated. The stability results are carried out at trimmed state with non zero flap deflection. The flap deflections are calculated by the coupled blade/flap/actuator equations. The actuator input, δ_0 , is set to zero, however, the flap deflection may not be zero. This is because a nonzero hinge moment exists even in the absence of a flap motion.

Baseline Rotor Correlation

The predictions of the stability characteristics of the baseline MDART bearingless rotor without trailing-edge flaps are compared with wind tunnel test data. Aeroelastic stability testing was conducted on the full-scale MDART rotor in the NASA Ames 40-by 80-foot wind tunnel in 1994. Figure 3 compares UMARC predictions of lag damping ratio with MDART test data in hover (Ref. 20). UMARC results agree well with the test data. Figure 4 illustrates lag damping variation of the MDART rotor with collective pitch for an advance ratio of 0.25. The shaft angle was set with a forward tilt of 7.3 degree that simulates a

steady level flight condition. UMARC results matched fairly well with the test data (Ref. 20).

The predictions of flap hinge moment is very important for the calculations of aeroelastic stability of a trailing-edge flap rotor because it directly determines the flap motion given the actuator input and couples the blade motion with the flap deflections. Because of lack of experiment data, the predictions of present analysis are correlated with another comprehensive code. Figure 5 compares flap hinge moment predictions from UMARC using table lookups as well as using analytical expressions with CAMRAD II predictions (Ref. 2). UMARC hinge moment predictions utilizing table lookup agree fairly with CAMRAD II results that are also calculated using table lookup. The predictions using Theodorsen flap model qualitatively agrees with the results using table lookup, however, there is a considerable under-prediction of the magnitude in the first quadrant. Figure 6 illustrates the flap response predictions with UMARC for an actuator input $\delta_a = 2^\circ \cos(4\psi - 240^\circ)$ at an advance ratio of 0.2. If the actuator is infinitely rigid, the flap response should be identical with the actuator input. Although the baseline actuator is relatively stiff, the half peak-to-peak flap response is 15% larger than the actuator input. This demonstrates the importance of including actuator dynamics in the model.

Trailing-edge flap aerodynamic balance

The effect of trailing-edge flap aerodynamic balance (nose overhang) is studied in this section, and the flap is assumed mass-balanced (flap mass CG is coincident

with the hinge). The purpose of implementing flap overhang is to reduce flap actuation requirements. Figure 7(a) shows that the actuation power was reduced by 60% with an overhang length of 29% of flap chord (hinge at 29% of flap chord) compared to the no overhang case (hinge at leading-edge of flap). Figure 7(b) shows that half peak-to-peak flap response increases with increasing overhang length, and more dramatically above 40% flap chord. Figure 8 illustrates the effect of flap overhang length on blade and trailing-edge flap stability characteristics. The trailing-edge flap mode damping decreases with increasing flap overhang, and becomes unstable with overhang length larger than 50% flap chord. This is because the flap becomes aerodynamically over-balanced with large flap overhang, and the flap mode diverges. The effects of flap overhang on blade stability results from the coupling between trailing-edge flap motion and blade modes. The trailing-edge flap is static mass-balanced in this case so that the coupling between flap and blade are primarily through aerodynamic forces. The aerodynamic coupling between blade flap mode and trailing-edge flap motion is in phase, that is positive trailing-edge flap deflection produces positive blade flap bending motion. This positive coupling results in a decrease in blade flap mode damping with increasing flap overhang. The aerodynamic coupling between blade torsion mode and trailing-edge flap mode is out of phase, that is positive trailing-edge flap motion decreases blade torsion motion. This negative coupling leads to an increase in blade torsion mode damping with increasing flap overhang. Blade lag mode virtually stays constant with flap overhang. It's shown that although aerodynamic balance of trailing-edge flap is the key to minimizing actuation

requirements, excessive overhang may lead to blade/trailing-edge flap instability.

Trailing-edge flap mass-balance

The effect of trailing-edge flap mass-balance on blade and trailing-edge flap stability is investigated in this section. The simulations were carried out with various flap CG offsets from the flap hinge, and this variation will change the inertia forces on the blade and trailing-edge flap. The flap CG offsets in this study are varied to show its sensitivity on stability. The baseline MD900 trailing-edge flap system is designed to be mass-balanced.

Figure 9(a) shows the variation of trailing-edge flap frequency with flap CG offset. The trailing-edge flap frequency is shown to decrease with increasing flap CG offset. This is because the moment of inertia of flap increases with flap CG offset and the actuator stiffness is kept same in this case. Figure 9(b) reveals the effect of flap CG offset on blade and trailing-edge flap stability characteristics. The trailing-edge flap mode is shown to become unstable after a flap CG offset of 0.26 flap chord. This instability is typical trailing-edge flap-blade torsion flutter. That instability results from the energy transfer between the trailing-edge flap mode and blade torsion mode. Blade flap mode damping is shown to decrease with flap CG offset and flap CG offset has a negligible effect on blade lag mode stability.

The study of various important blade and trailing-edge flap structural properties, such as rotor control stiffness, blade torsional stiffness, actuator stiffness, and trailing-edge flap size and locations are carried out in combination

with a mass-imbalanced flap (CG offset of 0.33 flap chord and flap overhang length of 0.29 flap chord). The simulations are conducted at advance ratio of 0.30 except where noted. Figure 10 shows the effect of rotor control system stiffness (designated as pitch link stiffness) on blade and trailing-edge flap stability characteristics. Figure 10(a) presents the variation of blade flap, lag, and torsion mode natural frequencies with pitch link stiffness. It shows that the blade torsion frequency increases from 2.3/rev for a pitch link stiffness of 158 lb/in to 4.2/rev for a pitch link stiffness of 800 lb/in. The blade flap and lag frequencies are essentially unchanged with pitch link stiffness. Figure 10(b) shows effect of pitch link stiffness on blade and trailing-edge flap stability characteristics. The flap overhang is 29% flap chord and the flap CG offset is 33% flap chord. The trailing-edge flap mode becomes gradually more unstable with increasing pitch link stiffness. Blade flap mode damping increases largely with pitch link stiffness whereas blade torsion mode damping slightly decreases. Blade lag mode damping shows small variation.

Figure 11 shows the effect of blade torsional stiffness (GJ factor over baseline value) on blade and trailing-edge flap stability. Figure 11(a) presents the variation of blade natural frequencies with blade GJ factor. The frequencies of blade flap and lag mode reveal virtually no variation with GJ factor while torsion frequency increases from 2.96/rev with 75% of the baseline GJ to 3.18/rev with twice the baseline GJ. Figure 11(b) presents the variation of blade and trailing-edge flap damping with GJ factor. Trailing-edge flap mode is unstable in the range from 75% to 200% baseline GJ, and shows small variation. Blade torsion mode

damping is shown to be slightly decreasing with increasing GJ factor whereas flap mode damping increases with GJ factor.

Figure 12 presents the effect of trailing-edge flap actuator stiffness on blade and trailing-edge flap stability characteristics. Figure 12(a) shows the variation of trailing-edge flap frequency with actuator stiffness for a mass-balanced flap (no flap CG offset) and a mass-imbalanced flap (flap CG offset of 33% flap chord). The frequencies of both types of flap increase largely with increasing actuator stiffness, however, the mass-imbalanced flap shows smaller variation slope than the mass-balanced flap because of its larger moment of inertia. Figure 12(b) illustrates the trailing-edge flap mode is unstable for the mass-imbalanced flap with a soft actuator, and becomes stable with actuator stiffness above 1.5 times the baseline actuator. Blade flap mode damping increases gradually with increasing actuator stiffness whereas torsional mode damping decreases. The effect of actuator stiffness on blade lag mode is negligible.

Figures 13, 14, and 15 examine the effect of trailing-edge flap size (length and chord ratio) and spanwise location on blade and trailing-edge flap stability characteristics. Figure 13 illustrates that trailing-edge flap mode becomes unstable when flap is positioned toward the blade tip. Blade flap mode damping is shown to decrease slightly with flap moving to blade tip, and torsion mode damping increases with flap placed toward tip. Blade lag mode damping shows no variation with trailing-edge flap location. Figure 14 shows that trailing-edge flap mode becomes unstable with flap length above 14% blade radius. Blade flap mode damping is shown to decrease with increasing flap length whereas torsion mode

increases with flap length. However, both modes are quite stable. Comparing figures 13 and 14, the flap length parameter is shown to have the similar effect as the flap location, though it is more effective at changing the blade and trailing-edge flap stability characteristics. Figure 15 shows trailing-edge flap mode is unstable with the flap chord in the range of 0.15 to 0.40 airfoil chord, and stable otherwise. This may be because of the aerodynamic characteristics of the trailing-edge flap changing dramatically with flap chord ratio. The flap pitching moment reaches a maximum around a flap chord ratio of 0.26, whilst the flap lift coefficients increase monotonically with flap chord ratio (Ref. 21). Again, because of the positive aerodynamic coupling between blade flap mode and trailing-edge flap motion, blade flap mode damping shows the same trends of variations as the trailing-edge flap mode with flap chord ratio. Conversely, the blade torsion mode damping presents the opposite pattern of variation with flap chord ratio comparing with trailing-edge flap mode because of the negative aerodynamic coupling between blade torsion mode and trailing-edge flap mode.

Figures 16 and 17 examine the variation of blade and trailing-edge flap stability characteristics in different flight conditions. Figure 16(a) shows the effect of blade collective pitch in hover. The trailing-edge flap mode is shown to become unstable with large collective pitch, though the variation is very small. Figure 16(b) shows the effect of blade collective pitch on blade and trailing-edge flap stabilities in forward flight condition with an advance ratio of 0.3. The trailing-edge flap mode is unstable in the range of collective pitch from four to twelve degrees, and is increasingly unstable with larger collective pitch. Figure 17

examines the effect of variation of forward speed. The trailing-edge flap mode is weakly unstable in hover and becomes more unstable with forward speed.

Conclusions

This paper examined the effects of various key design variables such as flap overhang length, flap CG offset, rotor control system stiffness, blade torsional stiffness, actuator stiffness, and trailing-edge flap size and location on the aeroelastic stability characteristics of a trailing-edge flap rotor system. Simulations for several advance ratios and various collective pitches were performed. The following conclusions are subject to the limitations of the analysis and the scope of the study:

1. Although flap aerodynamic balance (nose overhang) is a key to minimizing actuation requirements, excessive overhang may lead to blade/trailing-edge flap instability.
2. Large trailing-edge flap CG offsets cause torsion-flap flutter, especially at high advance ratios.
3. Increasing rotor control stiffness for a rotor with a mass-imbalanced flap may have a destabilizing effect on trailing-edge flap mode stability.
4. Increasing flap actuator stiffness for a rotor with a mass-imbalanced flap has a stabilizing effect on trailing-edge flap mode stability.

5. With a mass-imbalanced flap, increasing the flap length or moving flap toward blade tip has a destabilizing effect on trailing-edge flap mode stability.
6. Increasing collective pitch results in more instability of the trailing-edge flap mode.

Acknowledgments

The authors gratefully acknowledge Dr. Friedrich Straub (Boeing-Mesa) for making available the design data and experimental results as well as providing valuable advice and assistance. This work was supported by Boeing-Mesa under a DARPA contract.

References

¹Chopra, I., “Status of Application of Smart Structures Technology to Rotorcraft Systems,” *Journal of the American Helicopter Society*, Vol. 45, (4):228–252, October 2000.

²Straub, F. K. and Charles, B. D., “Aeroelastic Analysis of Rotors with Trailing Edge Flaps Using Comprehensive Codes,” *Journal of the American Helicopter Society*, Vol. 46, (3):192–199, July 2001.

³Prechtel, E. F. and Hall, S. R., “Design of a High Efficiency, Large Stroke,

Electromechanical Actuator,” *Smart Materials and Structures Journal*, Vol. 8, (1):13–30, February 1999.

⁴Fulton, M. V. and Ormiston, R. A., “Hover Testing of a Small-Scale Rotor with On-Blade Elevons,” *Journal of the American Helicopter Society*, Vol. 46, (2):96–106, April 2001.

⁵Koratkar, N. A. and Chopra, I., “Wind Tunnel Testing of a Mach-Scaled Rotor Model with Trailing-Edge Flaps,” *Journal of the American Helicopter Society*, Vol. 47, (4):263–272, October 2002.

⁶Bernhard, A. and Chopra, I., “Hover Test of a Mach-Scale Rotor Model with Active Blade Tips,” *Journal of the American Helicopter Society*, Vol. 47, (4):273–284, October 2002.

⁷Epps, J. J. and Chopra, I., “In-Flight Tracking of Helicopter Rotor Blades Using Shape Memory Alloy Actuators,” *Smart Materials and Structures Journal*, Vol. 10, (1):104–111, February 2001.

⁸Shen, J. and Chopra, I. “A Parametric Design Study for a Swashplateless Helicopter Rotor with Trailing-Edge Flaps,”. In *American Helicopter Society 58th Annual Forum Proceedings*, page 15, Montreal, Canada, June 11-13 2002.

⁹Chopra, I., “Perspectives in Aeromechanical Stability of Helicopter Rotors,” *Vertica*, Vol. 14, (4):457–508, 1990.

¹⁰Broadbent, E., “The Elementary Theory of Aero-Elasticity, Part III. Flutter of

Control Surfaces and Tabs,” *Aircraft Engineering*, Vol. 12, (13):145–153, May 1954.

¹¹Fung, Y., *An Introduction to the Theory of Aeroelasticity*, Dover Publications, Inc, 1993.

¹²Theodorsen, T. “General Theory of Aerodynamic Instability and the Mechanism of Flutter,” Technical Report No. 496, NACA, 1935.

¹³Bir, G., Chopra, I., et al. “University of Maryland Advanced Rotor Code (UMARC) Theory Manual,” Technical Report UM-AERO 94-18, Center for Rotorcraft Education and Research, University of Maryland, College Park, July 1994.

¹⁴Tracy, A. L. and Chopra, I., “Aeroelastic Analysis of a Composite Bearingless Rotor in Forward Flight Using a Improved Warping Model,” *Journal of the American Helicopter Society*, Vol. 40, (3):35–51, 1995.

¹⁵Hariharan, N. and Leishman, J. G. “Unsteady Aerodynamics of a Flapped Airfoil in Subsonic Flow by Indicial Concepts,”. In *Proceedings of the 36th AIAA/ASME/ASCE/AHS/ASC structure, structural dynamics, and materials conference*, New Orleans, LA, April 1995.

¹⁶Milgram, J., Chopra, I., and Straub, F., “Rotors with Trailing Edge Flaps: Analysis and Comparison with Experimental Data,” *Journal of the American Helicopter Society*, Vol. 43, (4):319–332, October 1998.

¹⁷Hassan, A. A., Straub, F. K., and Noonan, K. W. “Experimental/Numerical Evaluation of Integral Trailing Edge Flaps for Helicopter Rotor Applications,”. In *American Helicopter Society 56th Annual Forum Proceedings*, page 19, Virginia beach, VA, May 2-4 2000.

¹⁸Theodorsen, T. and Garrick, I. E. “Nonstationary Flow about a Wing-Aileron-Tab Combination Including Aerodynamic Balance,” Technical Report No. 736, NACA, 1942.

¹⁹Bagai, A. and Leishman, J. G., “Rotor Free-Wake Modeling Using a Pseudo-Implicit Technique - Including Comparisons with Experimental Data,” *Journal of the American Helicopter Society*, Vol. 40, (3), July 1995.

²⁰Nguyen, K., McNulty, M., Anand, V., and Lauzon, D. “Aeroelastic Stability of the McDonnell Douglas Advanced Bearingless Rotor,”. In *American Helicopter Society 49th Annual Forum Proceedings*, pages 1283–1290, St. Louis, MO, May 19-21 1993.

²¹Hoerner, S. F. and Borst, H. V. *Fluid-Dynamic Lift*, chapter Characteristics of Airplane Control Surfaces. Hoerner fluid dynamics, 1975.

Table 1: MDART Rotor and Flap Properties

Rotor Data

Rotor Type	Bearingless
Number of Blades	5
Rotor Diameter	34 ft
Rotor Speed	392 RPM
Chord	10 in
Lock Number	9.17
Solidity	0.078

Flap and Actuator Data

Flap Type	Plain Flap
Spanwise Length	36 inch (18%R)
Chordwise Size	35 % (Blade Chord)
Flap Midspan Location	83% R
Flap Hinge Overhang	29% (Flap Chord)
Actuator Stiffness	81.52 (ft-lb/rad)
Actuator Damping	0.005 (ft-lb/rad/sec)

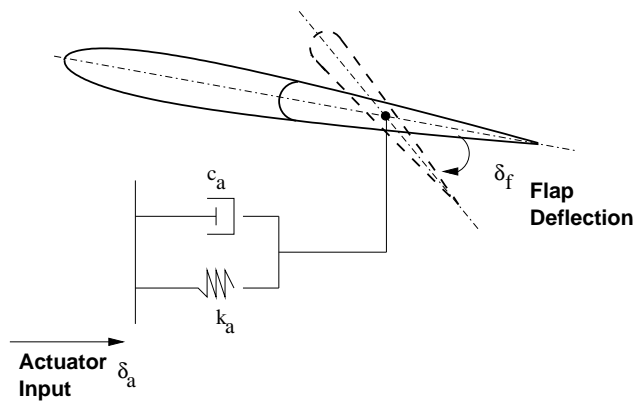


Figure 1: Actuator and Flap System

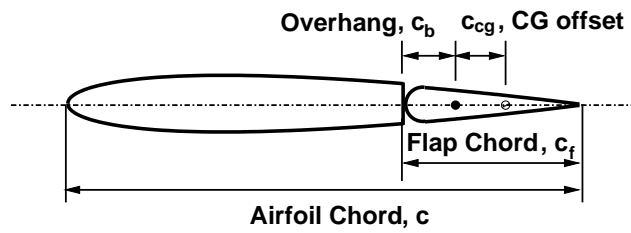


Figure 2: Trailing-edge flap with aerodynamic balance (nose overhang)

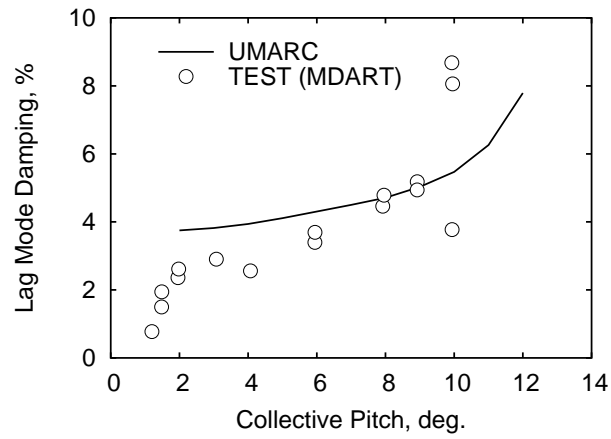


Figure 3: Blade inplane stability in hover for the baseline rotor (without trailing-edge flaps)

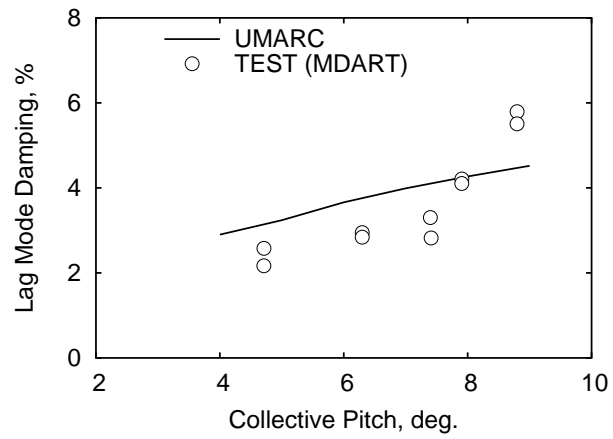


Figure 4: Blade inplane stability in forward flight for the baseline rotor (without trailing-edge flaps), $\mu = 0.25$, forward shaft tilt of 7.3 degree

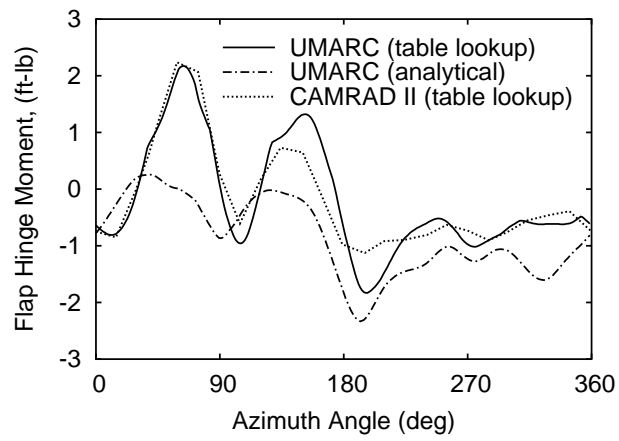


Figure 5: Flap hinge moment in one complete revolution, with prescribed flap motion $\delta_f = 2^\circ \cos(4\psi - 240^\circ)$, $\mu = 0.2$, $C_T/\sigma = 0.0774$, $c_b/c_f = 0.29$, $c_{cg}/c_f = 0$

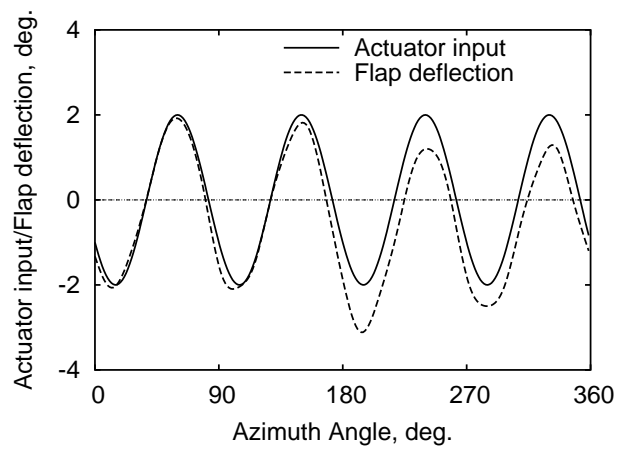
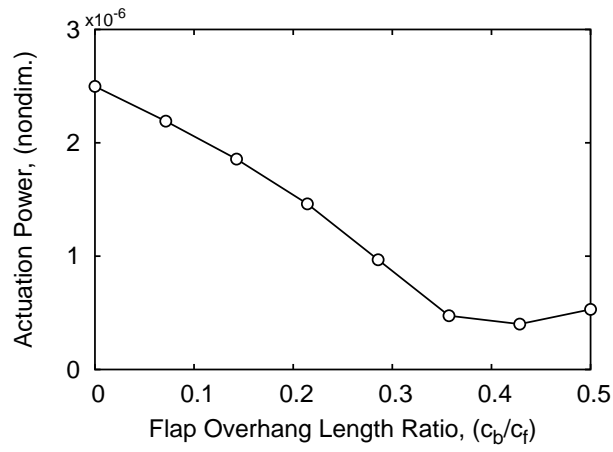
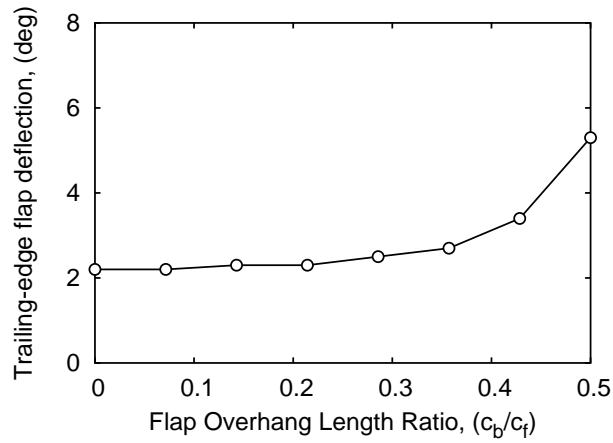


Figure 6: Trailing-edge flap response with actuator input $\delta_a = 2^\circ \cos(4\psi - 240^\circ)$, $\mu = 0.2$, $C_T/\sigma = 0.0774$, $c_b/c_f = 0.29$, $c_{cg}/c_f = 0$



(a) Actuation requirement



(b) Trailing-edge flap response

Figure 7: Trailing-edge flap actuation power and response (half peak-to-peak) versus trailing-edge flap overhang length, $\mu = 0.2$, $C_T/\sigma = 0.0774$, $c_{cg}/c_f = 0$, $\delta_a = 2^\circ \cos(4\psi - 240^\circ)$

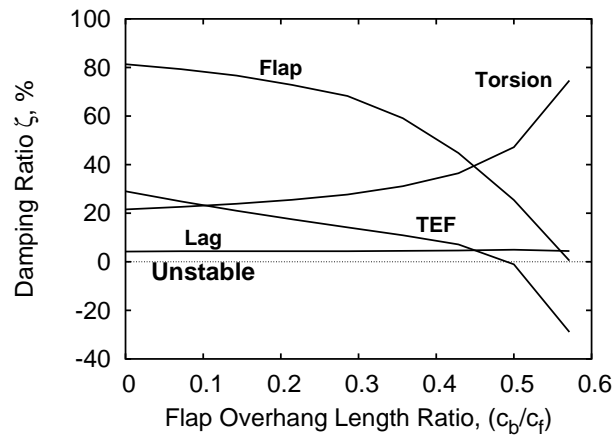
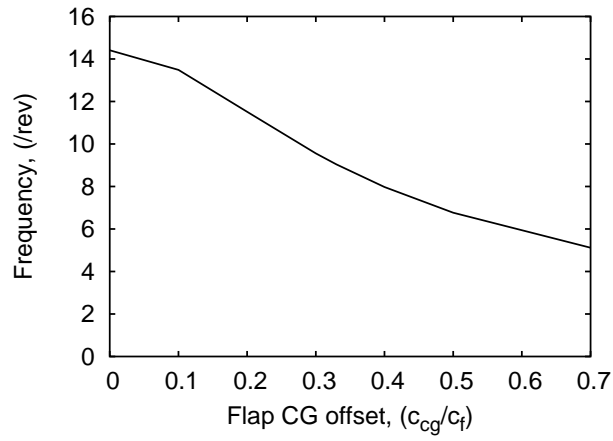
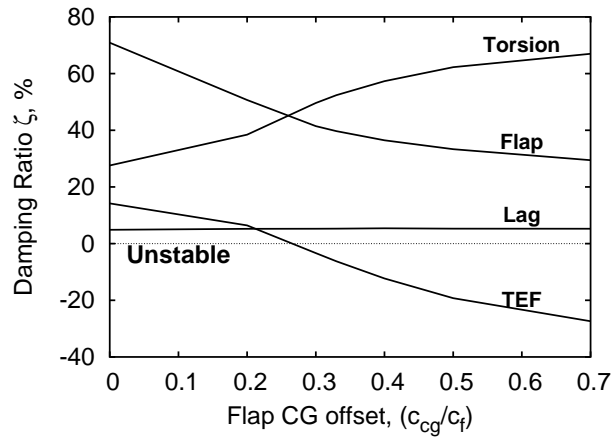


Figure 8: Effect of overhang length on blade and trailing-edge flap (TEF) stability in hover, $c_{cg}/c_f = 0$

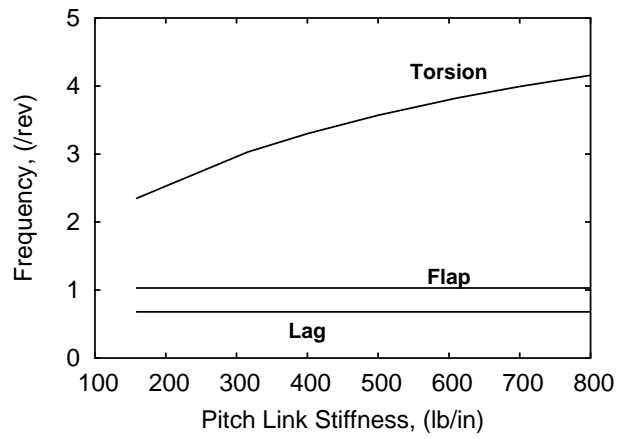


(a) Trailing-edge flap frequency

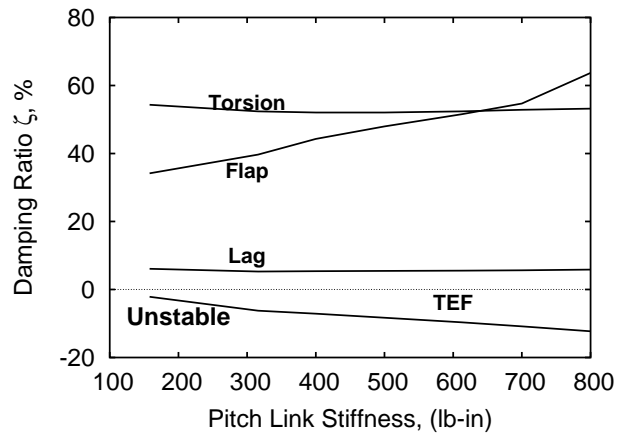


(b) Blade and trailing-edge flap damping

Figure 9: Effect of flap CG offset on blade and trailing-edge flap (TEF) stability in forward flight, $c_b/c_f = 0.29$, $\mu = 0.30$

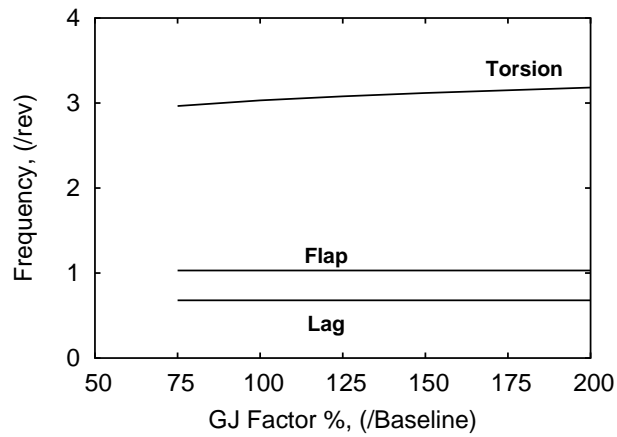


(a) Blade frequency

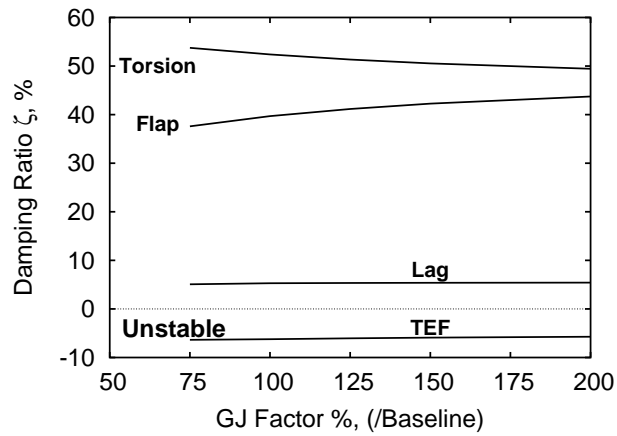


(b) Blade and trailing-edge flap damping

Figure 10: Effect of pitch link stiffness on blade and trailing-edge flap (TEF) stability in forward flight, $\mu = 0.30$, $c_b/c_f = 0.29$, $c_{cg}/c_f = 0.33$

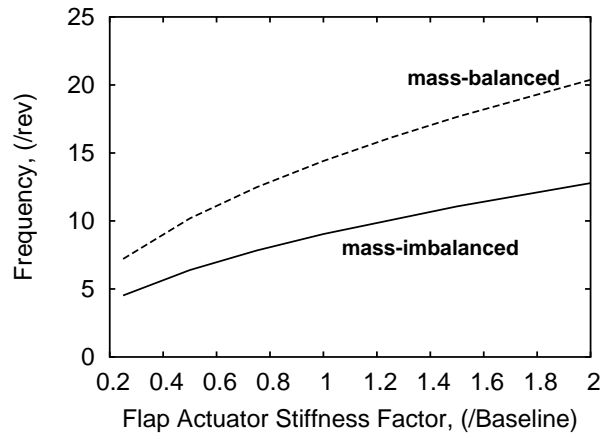


(a) Blade frequency

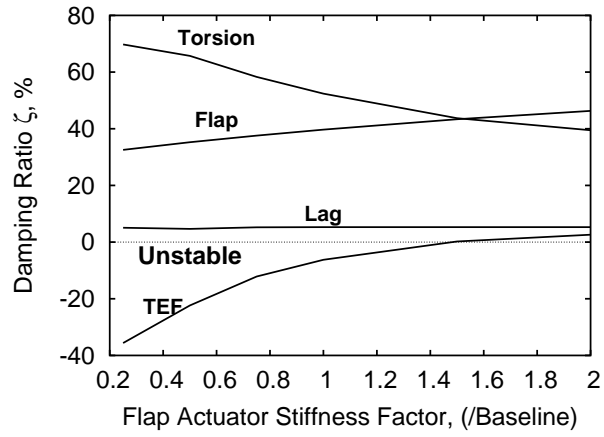


(b) Blade and trailing-edge flap damping

Figure 11: Effect of blade torsional stiffness on blade and trailing-edge flap (TEF) stability in forward flight, $\mu = 0.30$, $c_b/c_f = 0.29$, $c_{cg}/c_f = 0.33$



(a) Trailing-edge flap frequency



(b) Blade and trailing-edge flap damping, $c_{cg}/c_f = 0.33$

Figure 12: Effect of actuator stiffness on blade and trailing-edge flap (TEF) stability in forward flight, $\mu = 0.30$, $c_b/c_f = 0.29$

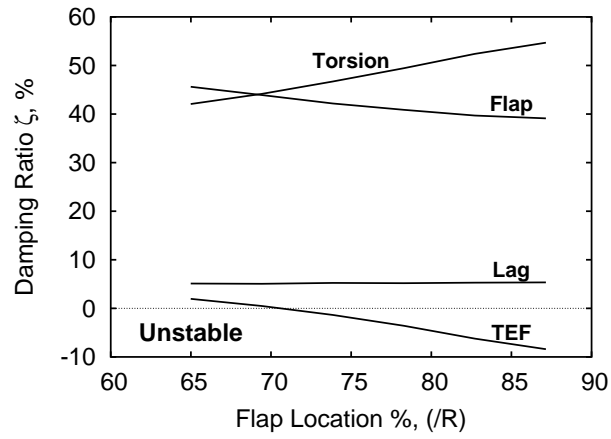


Figure 13: Effect of flap spanwise location on blade and trailing-edge flap (TEF) stability in forward flight, $\mu = 0.30$, $c_b/c_f = 0.29$, $c_{cg}/c_f = 0.33$

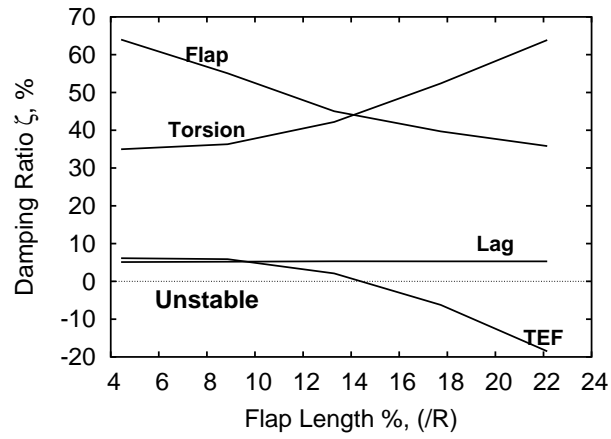


Figure 14: Effect of flap length on blade and trailing-edge flap (TEF) stability in forward flight, $\mu = 0.30$, $c_b/c_f = 0.29$, $c_{cg}/c_f = 0.33$

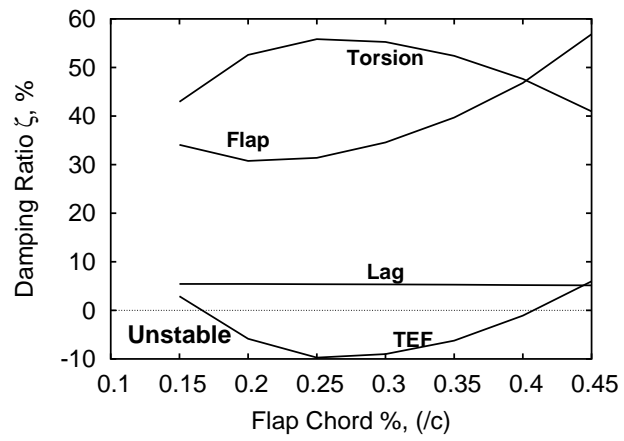
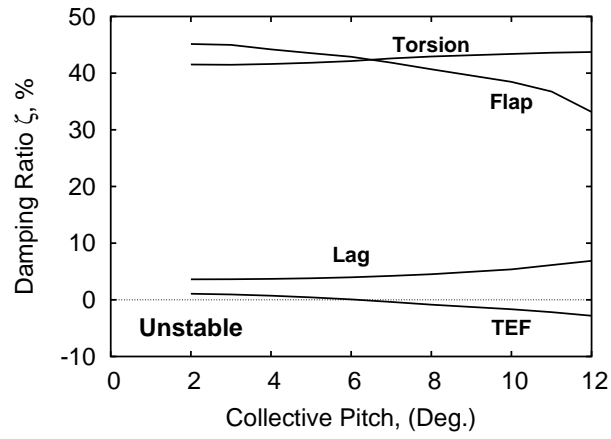
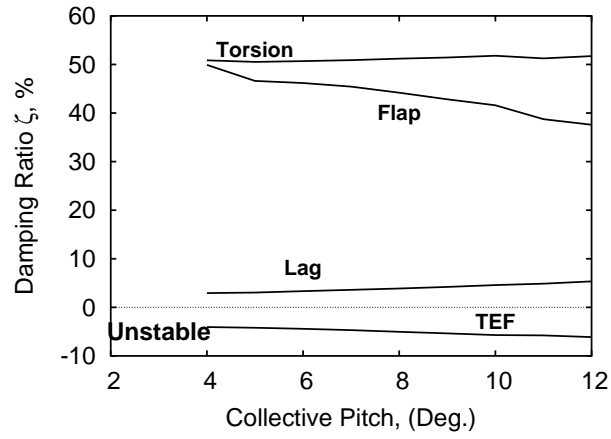


Figure 15: Effect of flap chord size on blade and trailing-edge flap (TEF) stability in forward flight, $\mu = 0.30$, $c_b/c_f = 0.29$, $c_{cg}/c_f = 0.33$



(a) Hover



(b) Forward flight, $\mu = 0.30$

Figure 16: Effect of collective pitch on blade and trailing-edge flap (TEF) stability, $c_b/c_f = 0.29$, $c_{cg}/c_f = 0.33$

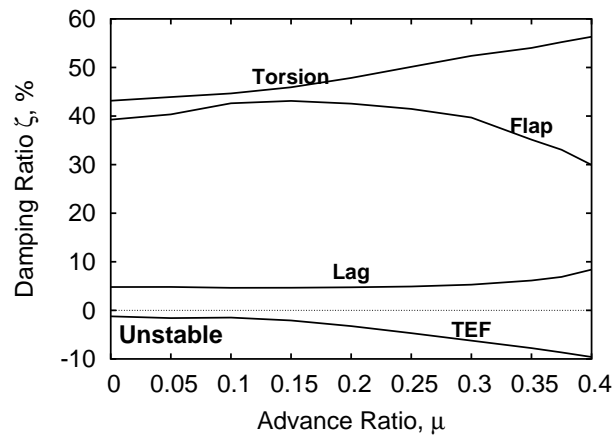


Figure 17: Effect of forward speed on blade and trailing-edge flap (TEF) stability, $c_b/c_f = 0.29$, $c_{cg}/c_f = 0.33$

List of Figures

1	Actuator and Flap System	24
2	Trailing-edge flap with aerodynamic balance (nose overhang) . . .	25
3	Blade inplane stability in hover for the baseline rotor (without trailing-edge flaps)	26
4	Blade inplane stability in forward flight for the baseline rotor (without trailing-edge flaps), $\mu = 0.25$, forward shaft tilt of 7.3 degree	27
5	Flap hinge moment in one complete revolution, with prescribed flap motion $\delta_f = 2^\circ \cos(4\psi - 240^\circ)$, $\mu = 0.2$, $C_T/\sigma = 0.0774$, $c_b/c_f = 0.29$, $c_{cg}/c_f = 0$	28
6	Trailing-edge flap response with actuator input $\delta_a = 2^\circ \cos(4\psi - 240^\circ)$, $\mu = 0.2$, $C_T/\sigma = 0.0774$, $c_b/c_f = 0.29$, $c_{cg}/c_f = 0$	29
7	Trailing-edge flap actuation power and response (half peak-to-peak) versus trailing-edge flap overhang length, $\mu = 0.2$, $C_T/\sigma = 0.0774$, $c_{cg}/c_f = 0$, $\delta_a = 2^\circ \cos(4\psi - 240^\circ)$	30
8	Effect of overhang length on blade and trailing-edge flap (TEF) stability in hover, $c_{cg}/c_f = 0$	31
9	Effect of flap CG offset on blade and trailing-edge flap (TEF) stability in forward flight, $c_b/c_f = 0.29$, $\mu = 0.30$	32
10	Effect of pitch link stiffness on blade and trailing-edge flap (TEF) stability in forward flight, $\mu = 0.30$, $c_b/c_f = 0.29$, $c_{cg}/c_f = 0.33$	33

11	Effect of blade torsional stiffness on blade and trailing-edge flap (TEF) stability in forward flight, $\mu = 0.30$, $c_b/c_f = 0.29$, $c_{cg}/c_f = 0.33$	34
12	Effect of actuator stiffness on blade and trailing-edge flap (TEF) stability in forward flight, $\mu = 0.30$, $c_b/c_f = 0.29$	35
13	Effect of flap spanwise location on blade and trailing-edge flap (TEF) stability in forward flight, $\mu = 0.30$, $c_b/c_f = 0.29$, $c_{cg}/c_f = 0.33$	36
14	Effect of flap length on blade and trailing-edge flap (TEF) stability in forward flight, $\mu = 0.30$, $c_b/c_f = 0.29$, $c_{cg}/c_f = 0.33$	37
15	Effect of flap chord size on blade and trailing-edge flap (TEF) stability in forward flight, $\mu = 0.30$, $c_b/c_f = 0.29$, $c_{cg}/c_f = 0.33$	38
16	Effect of collective pitch on blade and trailing-edge flap (TEF) stability, $c_b/c_f = 0.29$, $c_{cg}/c_f = 0.33$	39
17	Effect of forward speed on blade and trailing-edge flap (TEF) stability, $c_b/c_f = 0.29$, $c_{cg}/c_f = 0.33$	40

List of Tables

1	MDART Rotor and Flap Properties	23
---	-------------------------------------------	----